Evidence for a compact σ^{70} conformation *in vitro* and *in vivo*

Khalil Joron[1], Joanna Zamel[1], Nir Kalisman[1,2], Eitan Lerner[1,2]*

Affiliations

[1] Department of Biological Chemistry, Alexander Silberman Institute of Life Sciences, Faculty of Mathematics & Science, Edmond J. Safra Campus, Hebrew University of Jerusalem; Jerusalem 9190401, Israel.

[2] Center for Nanoscience and Nanotechnology, Hebrew University of Jerusalem; Jerusalem 9190401, Israel.

* Corresponding author email: eitan.lerner@mail.huji.ac.il

Abstract

The initiation of transcription in Escherichia coli (*E. coli*) is facilitated by promoter specificity factors, also known as σ factors, which may bind a promoter only as part of a complex with RNA polymerase (RNAP). By performing *in vitro* cross-linking mass spectrometry (CL-MS) of apo-σ^{70}, we reveal structural features suggesting a compact conformation compared to the known RNAP-bound extended conformation. Then, we validate the existence of the compact conformation using *in vivo* CL-MS by identifying cross-links similar to those found *in vitro*, which deviate from the extended conformation only during the stationary phase of bacterial growth. Conclusively, we provide information in support of a compact conformation of apo-σ^{70} that exists in live cells, which might represent a transcriptionally-inactive form that can be activated upon binding to RNAP.

Keywords: σ^{70}, transcription, cross-linking mass spectrometry, RNA polymerase.

Introduction

σ promoter specificity factors facilitate the specific binding of RNAP to gene promoters in bacteria[1,2]. Among the different types of σ factors in *E. coli*, σ^{70} binds promoters of house-keeping genes under optimal conditions at the logarithmic phase of bacterial growth[3]. The mechanism of initiating DNA transcription involves the binding of σ^{70} to dsDNA promoter only when σ^{70} is bound to the core RNAP complex[4]. In the RNAP complex, σ^{70} is found in a unique structural organization, in which σ^{70} regions 2 and 4 (σR2 and σR4, respectively) are distant from each other[4], to expose its DNA-binding residues, and by that facilitate transcription initiation[5]. The formation of the RNAP-promoter closed (RP_C) complex is followed by a cascade of DNA isomerization events[6–10], which end with a stretch of 10-12 melted bases of promoter DNA upstream to the transcription start site, which forms the DNA transcription bubble, that is later stabilized in the RNAP-promoter open (RP_O) complex[11,12]. Importantly, throughout transcription initiation σ^{70} remains part of the holoenzyme complex and retains the extended conformation. Nonetheless, as all parts of the transcription initiation complex, including σ^{70}, are translated and formed separately, σ^{70} may exist in bacteria also in an unbound apo form, at least as long as it is not bound to RNAP. Apo-σ^{70} can also bind anti-σ factors, which repress transcription by competing with RNAP on the interaction with σ^{70}, and even by sequestering σ^{70} out of the cytoplasm[13–15]. However, different factors may lead to the release of σ^{70} from its interaction with anti-σ factors, and back into the cytoplasm, until it rebinds RNAP[16–19]. Therefore, this process, among others, might dictate the lifetime in which σ^{70} exists in an unbound apo form.

Structurally, the protein data bank (PDB) includes many entries of high-resolution structures of transcription initiation complexes, where σ^{70} is present as a subunit[4,8,20–30]. Exploring the PDB for apo-σ^{70} identifies only a few *E. coli*-related structures of its separate regions, such as σ^{70} region 4 (i.e., σR4) bound to several transcription factors[31–33], the unbound σ^{70} region 2 (i.e., σR2)[34,35], as well as structures of regions in house-keeping σ factors from bacteria other than *E. coli*[35,36]. However, a structural description of full-length apo-σ^{70} has not yet been reported. Nevertheless, previous *in vitro* biochemical works showed that apo-σ^{70} adopts a predominant distinct compact conformation[37–40], which can undergo an overall structural reorganization upon binding core RNAP. Binding induces a conformational change from an unbound compact state to a RNAP-bound extended state[41–45].

In this work, we provide evidence for the existence of the compact apo-σ^{70} conformation both *in vitro* and *in vivo*. First, we perform *in vitro* single-molecule Förster resonance energy transfer (smFRET)[46,47] experiments to verify that apo-σ^{70} is found predominantly in a compact conformation. Moreover, we also find that the presence of a promoter DNA alone (i.e., in the absence of RNAP) can induce only a minor population shift towards the extended conformation of σ^{70}. Relying on smFRET data, we further study the structural features of apo-σ^{70} by performing *in vitro* cross-linking mass-spectrometry (CL-MS) [48–53]. Comparison of the resolved residue proximities against the PDB full-length σ^{70} structures confirms the description of apo-σ^{70} as having a compact conformation. Furthermore, we show a global decrease in the distance between σR2 and σR4, which could support a DNA-binding auto-inhibitory mechanism, for preventing DNA binding not in the context of transcription.

Finally, results from *in vivo* CL-MS experiments on σ^{70} in *E. coli*, report the abundance of inter-residue proximities that cannot be explained by the extended σ^{70} PDB structures. Interestingly, the compact apo-σ^{70} conformation exists not in the logarithmic bacterial growth phase when σ^{70} is recruited for

transcription, but rather in the stationary phase when alternative σ factors are recruited for transcription to replace σ^{70}.

***In vitro* single-molecule FRET of apo-σ^{70} reveals a predominant compact conformation**

To study the inter-region conformational dynamics of σ^{70}, we doubly labeled σR2 and σR4 with fluorescent dyes for smFRET measurements, as shown before[37](see Methods). Importantly, using an smFRET hybridizing probe-based transcription assay, presented previously by Weiss and co-workers[54,55], we show that both the *wt* and the mutant used for dye-labeling are transcriptionally-active (Fig. S1). The double-labeled σ^{70} has an expected FRET efficiency of ~0.5 when it is a subunit of the RNAP holoenzyme structure[5]. SmFRET measurements result in a predominant FRET sub-population with higher FRET efficiency (Fig. 1, a-c), which point towards a conformation of σ^{70} where regions 2 and 4 are in close proximity, consistent with previously published data of similar smFRET measurements[5]. Further, we report the distribution of raw FRET values (E_{raw}) of single σ^{70} molecules, probed for freely-diffusing molecules through a confocal spot within few ms, in which they can undergo conformational changes at the diffusion timescale or faster. To report the underlying conformational states and the potential within-burst conformational dynamics, we analyze the smFRET burst data using multi-parameter photon-by-photon hidden Markov modeling (mpH^{2}MM)[56] (Fig. 1, d-f). Apo-σ^{70} transitions between four sub-populations, with one being an acceptor-photoblinked sub-population, and hence does not report FRET-relevant information (Fig. 1, d, purple dots), and three more sub-populations with both donor and acceptor fluorescently-active (Fig. 1, d, blue, red and green dots). The rates of the transitions between the three FRET sub-populations are in the ms timescale, where only rates of 20 s^{-1} or higher can be considered as arising from within-burst dynamics recorded in the experiment, due to burst durations of 50 ms at most (Table S1). Two out of the three FRET sub-populations exhibit almost equal mean E_{raw} values (Fig. 1, d, black dots within the group of blue and red dots) and together represent one predominant FRET sub-population (Fig. 1, d, blue and red dots). The third minorly-populated FRET sub-population (Fig. 1, d, green dots) exhibits a slightly lower mean E_{raw} (Fig. 1, d, black dot within the group of green dots). These results suggest a predominant compact σ^{70} conformation and a minorly-populated slightly-less compact σ^{70} conformation. Incubating the dye-labeled apo-σ^{70} in the presence of 2 µM dsDNA *lacCONS*[54,57] promoter (Fig. 1, c, f), gives rise to a small fraction of σ^{70} molecules in a FRET sub-population (Fig. 1, f, green dots) at lower mean E_{raw} (Fig. 1, f, black dot within the group of green dots) compared to the same minorly-populated sub-population in apo-σ^{70}. These results correspond to a further increase in the distance between σR2 and σR4 for a low fraction of σ^{70} molecules, whereas the majority of apo-σ^{70} stay in the high FRET sub-population. In the presence of lower concentration of dsDNA *lacCONS* promoter (100 nM; Fig. 1, b, e), this minorly-populated sub-population decreases to values similar to those in the absence of dsDNA (as seen relative to Fig. 1, a). Notably, the dsDNA *lacCONS* promoter should bind σ^{70}, when it is a subunit of the RNAP holoenzyme[57,58]. Indeed, in previous smFRET studies involving σ^{70} a full shift towards lower FRET values occurred in the presence of only a few nM of dsDNA, only when in the presence of RNAP[9,10]. Therefore, a small fraction of apo-σ^{70} molecules can undergo a small conformational change in the presence of µM concentrations of dsDNA. The transition rates from the predominant compact conformation represented by the high FRET sub-populations (blue and red) to the slightly-less compact sub-population (green), are in the tens of ms, and become as slow as hundreds of ms in the presence of dsDNA (Table S1). It is important to remember, however, that transition rates slower than 20 s^{-1} only point towards the inability of mpH^{2}MM to resolve the slow conformational dynamics in these cases.

Overall, the results of the *in vitro* smFRET measurements suggest that apo-σ^{70} is in an equilibrium between two states, a predominant compact conformation and a minorly-populated slightly less compact

conformation that is still more compact than the fully-extended-RNAP-bound σ^{70}, which is well-described by PDB structures. Therefore, we can assume that C_α-C_α distances between σR2 and σR4 in the predominant conformation of apo-σ^{70} may yield the short proximities that allow cross-linking to occur efficiently. Thus, we set out to describe the structural features of the apo-σ^{70} compact conformation using *in vitro* CL-MS.

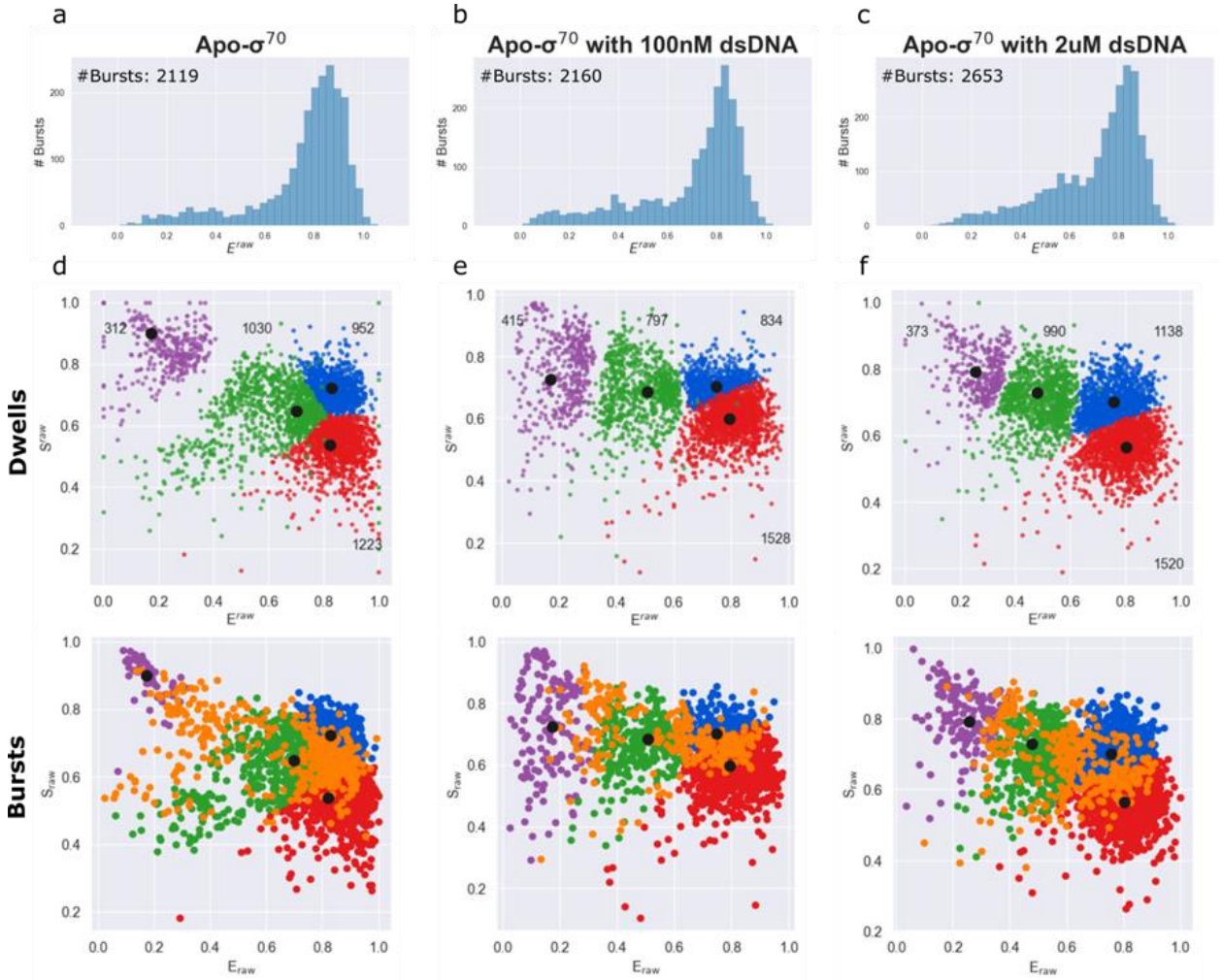

Fig. 1. SmFRET analyses of apo-σ^{70} conformations in the absence and presence of promoter dsDNA

(**a-c**) smFRET burst analysis (**d-f**) mpH^{2}MM analysis of σ^{70} labeled at residues 442 and 579 with ATTO 550 and ATTO 643, respectively. (**a**) Apo-σ^{70}, a major population exists at high raw FRET efficiencies, $E_{raw,}$ with a tail towards lower E_{raw} values. (**b**) Apo-σ^{70} with 100 nM dsDNA, exhibits no significant change in the major E_{raw} population. (**c**) Apo-σ^{70} with 2 µM dsDNA, exhibits a slight increase in sub-population with lower E_{raw}. (**d-f**) Dwells in states within bursts, (dwell-based analysis; top) and burst-based analysis (bottom), where different sub-populations in different states are shown in blue, red, green and magenta, and the bursts that include transitions between states are shown in orange. (**d**) Apo-σ^{70} – the predominant sub-populations (blue and red) of the compact conformation exhibit dynamics to a minor sub-population (green) of a less compact conformation. (**e**) σ^{70} in the presence of 100 nM dsDNA – the green sub-population is shifted, relative to (d), towards lower mean E_{raw} values suggesting binding to dsDNA influences the conformation of a minor sub-population in σ^{70}, while (**f**) in the presence of 2 µM dsDNA shows a higher an increase in the population of the green sub-population, suggesting the dsDNA-bound σ^{70} occurs more often at µM concentrations, yet most of σ^{70} still remains in the high E_{raw} sub-population (in the compact conformation; blue and red). Transition times between the blue or red sub-populations and the green sub-population, and vice versa, are in a few to tens of

ms, in the absence or presence of dsDNA. The magenta sub-population can be best described by a pure donor-only sub-population shown using uncorrected raw FRET and ALEX data (E_{raw} and S_{raw}).

Structural features of the unique compact apo-σ^{70} conformation using *in vitro* CL-MS

We perform *in vitro* cross-linking of purified recombinant *wt* apo-σ^{70} with either a zero-length primary amine to carboxyl coupler, 4-(4,6-dimethoxy-1,3,5-triazin-2-yl)-4-methyl-morpholinium chloride (DMTMM)[50], or a primary amine to primary amine cross-linker, bis(sulfosuccinimidyl)-substrate (BS^3)[59]. The cross-linked sample is then digested with trypsin and analyzed using MS (for further information, see Supplementary Information). We attain both short and intermediate scale spatial information, which report the C_α-C_α distances that are <16 or <30 Å for DMTMM and BS^3, respectively (Table 1). We show that without cross-linking the majority of σ^{70} (~66%) is in a monomeric form, while the rest exists as higher-order species (Fig. S2, a). As a result of cross-linking, the fraction of monomeric σ^{70} decreases by 6%, without affecting the overall layout of the eluted peaks (Fig. S2, b). Therefore, we suggest that many of the cross-links we achieve originate from the monomeric form. After false detection rate (FDR)-based data filtration (Fig. S3, a & b) according to the fragmentation score of each cross-linked peptide (see Supplementary Information), the highest-ranking cross-links are summarized in supplementary spreadsheet. We test the satisfaction rate of the recovered C_α-C_α distances against the same pairs of residues in existing PDB structures of σ^{70} (Table S2). The interconnectivity between σ^{70} regions (Fig. S4), include pairs of cross-linked residues between σ^{70} regions that are expected to be distant from each other (e.g., σR2 and σR4) and should not generate distances within the distance cutoffs of the cross-linkers used, if based on spatial information given by all PDB structures. Since all existing PDB structures of σ^{70} possess similar features and are almost identical, we display the recovered cross-links using one representative PDB structure of σ^{70} in the RNAP holoenzyme complex (6P1K)[25] (Fig. 2, a & b), and summarize the results for all PDB structures in a table (Table 1). Out of this comparison, we infer that 43-46% of the BS^3 and 25-38% of the DMTMM cross-links are satisfied and fit well within the structural coordinates of the pairs of residues. According to PDB structures coordinates most cross-links exceed the C_α-C_α distance range covered by the cross-linkers, suggesting that the PDB structures do not represent all possible monomeric conformations captured in solution during cross-linking. Next, we perform modeling using AlphaFold2[60,61] and RoseTTAFold[62], to test whether the expected compact conformation may be predicted via training and based on previously acquired structural data alone. AlphaFold2 was able to predict a more compact conformation than the one present in the PDB (Fig. 3, a-c). Yet, predicted models retain a high violation percentage of the cross-linking data (Table S2, and Fig. 3, d & e), suggesting a more compact conformation of apo-σ^{70} exists and is not available in the structural database, which the algorithms were trained on. The relatively low predicted local distance difference test score of σR3 and σR4 (Fig 3, a), suggest that a more compact conformation which the algorithm was not able to predict may exist. According to the residue-residue alignment confidence plot (Fig. 3, b), the interaction of the σR2/σR3 with σR4 is missing in the AlphaFold2 models, contrary to CL-MS results. Next, we test the satisfaction rate of CL-MS data against the predicted structure models, and find a similar level of satisfaction with up to 36% and up to 50% for the DMTMM and BS^3 data, respectively (Table S2). Overall, across all PDB structures and predicted structure models of σ^{70}, we detect the same cross-linked pairs of residues that cannot be explained by the spatial distances given in these structures. Interestingly, these unique pairs of cross-linked residues include mostly ones connecting σR2/σR3 with σR4 (Table 1), which are the primary DNA-binding regions.

Table 1. List of pairs of residues recovered from apo-σ^{70} *in vitro* CL-MS.

BS^3 and DMTMM cross-linked pairs of residues recovered from cross-linking mass spectrometry. Residues are assigned to their originating regions: σ region 1.2 (σR1.2), σ non-essential region (σNER), σ region 2 (σR2), σ region 3 (σR3), and σ region 4 (σR4). Residue numbering is according to the sequence given by the PDB structure 6P1K. Blue/Red/Black - residues that satisfy the pair-of-residue C_α-C_α distance given by the PDB structure, residues that violate the distance and unstructured residues in the PDB structure, respectively.

BS^3			BS^3			DMTMM		
Regions	**Residue #1**	**Residue #2**	**Regions**	**Residue #1**	**Residue #2**	**Regions**	**Residue #1**	**Residue #2**
σR1.2-σNER	K121	K257	σNER-σR4	K343	K593	σR1.2	T107	E104
σR.12-σNER	K121	K264	σNER-σR4	K264	K593	σR1.2-σR2	D96	K376
σR1.2-σNER	K121	K238	σNER-σR4	K236	K578	σR1.2-σR2	E104	K371
σR1.2-σNER	K121	S241	σNER-σR4	K257	K593	σR1.2-σR2	E104	S389
σR1.2-σNER	K121	K220	σR2	K371	K377	σR1.2-σR2	E109	K426
σR1.2-σR2	K121	K371	σR2	K371	K376	σR1.2-σR2	D125	K371
σR1.2-σR2	K121	K426	σR2-σR3	K371	K462	σR1.2-σR3	E109	K462
σ1.2-σR3	K121	K462	σR2-σR3	K393	K462	σNER	K236	E335
σR1.2-σR4	K121	K578	σR2-σR3	K418	K462	σNER	K236	E247
σNER	K220	K251	σR2-σR3	K377	K462	σNER	E152	K257
σNER	K220	K264	σR2-σR4	K377	S604	σNER	K296	D332
σNER	K257	K264	σR2-σR4	K371	K578	σNER-σR4	E343	D613
σNER	K238	T244	σR2-σR4	K377	K557	σNER-σR4	E247	K557
σNER	K236	K264	σR2-σR4	K377	K593	σNER-σR4	E349	K593
σNER	K220	K257	σR2-σR4	K392	K593	σR2	E407	S442
σNER	K236	K251	σR2-σR4	K377	K578	σR2-σR3	D445	K462
σNER	K289	K343	σR3	K462	K496	σR2-σR4	K376	D613
σNER	K238	S241	σR3	K462	K493	σR2-σR4	K392	D546
σNER	K251	K264	σR3-σR4	K462	K557	σR3	K462	E491
σNER	Y228	K236	σR3-σR4	K462	K593	σR3-σR4	K462	D546
σNER	K236	K257	σR3-σR4	K462	S604	σR3-σR4	K493	D546
σNER	Y228	K257	σR3-σR4	K462	K578	σR3-σR4	K493	D613
σNER	K220	S253	σR3-σR4	K493	K557	σR3-σR4	K462	D613
σNER-σR2	K257	K371	σR3-σR4	K496	K557	σR4	D546	K557
σNER-σR2	K264	K371	σR3-σR4	K493	Y571	σR4	D546	K593
σNER-σR2	K264	K418	σR3-σR4	K496	K593	σR3-σR4	K462	D613
σNER-σR2	K236	K371	σR3-σR4	K493	K593	σR4	D546	K557
σNER-σR2	K343	K371	σR4	K578	K593	σR4	D546	K593
σNER-σR2	K220	K371	σR4	Y571	K593			
σNER-σR2	K264	K377	σR4	K593	K597			
σNER-σR3	K220	K462						
σNER-σR3	K257	K462						
σNER-σR3	K264	K462						
σNER-σR3	K220	K493						
σNER-σR3	K343	K462						
σNER-σR3	K236	K462						
σNER-σR3	S241	K493						
σNER-σR3	K264	K496						

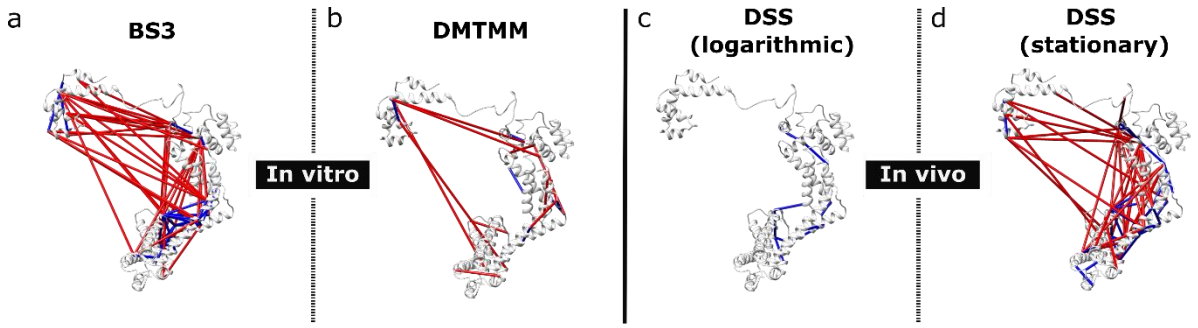

Fig. 2. Apo-σ^{70} *in vitro* and *in vivo* distances recovered from CL-MS suggest a compact conformation exists in solution and during stationary phase of bacterial growth. The RNAP-bound σ^{70} conformation from PDB structure (6P1K). (**a**) *In vitro* BS^3 and (**b**) DMTMM cross-links. (**c)** *In vivo* DSS cross-links at logarithmic growth phase. (**d**) *In vivo* DSS cross-links at stationary growth phase. Blue and red – cross-links recovered distances that are within or are not within the C_α-C_α distance covered by the crosslinker, respectively.

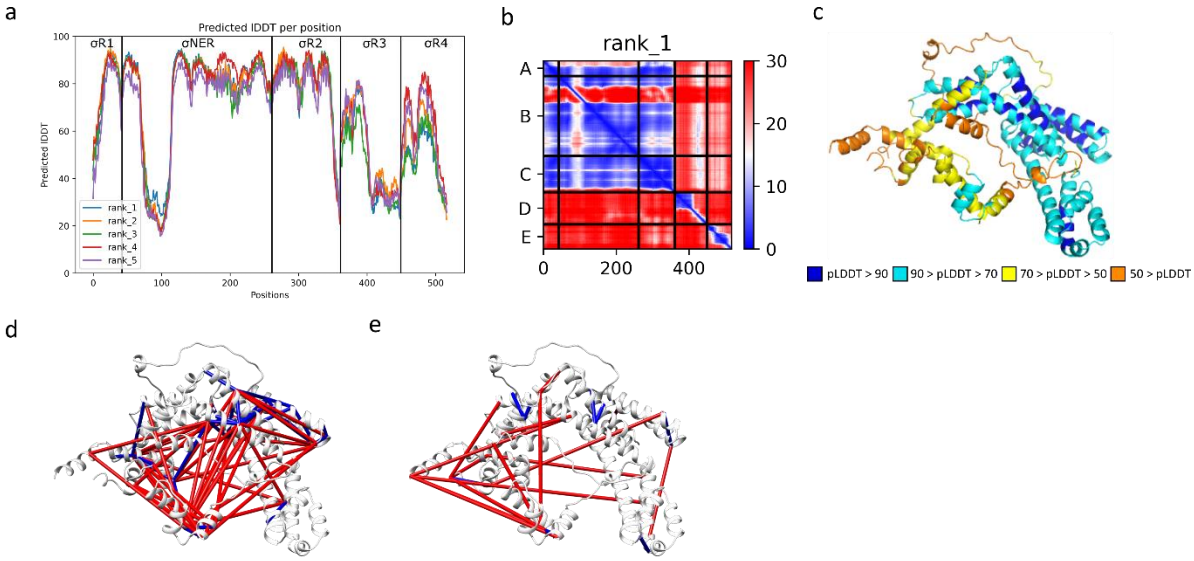

Fig. 3. AlphaFold2 Multimer predicts a compact conformation which does not satisfy CL-MS data. (**a**) Predicted pLDDT (AlphaFold2 output) for each residue in the top 5 predicted model structures. While the domains are predicted with high LDDT, linkers are significantly lower in their values. σ^{70} domains are separated in different boxes. (**b**) Predicted inter-residue interactions of the top-ranking model, where A, B, C, D and E correspond to σR1, σNER, σR2, σR3 and σR4, respectively. Blue color indicates that interaction occurred between the two regions, while red color indicates no interaction. (**c**) Rank 1 relaxed model is in a more compact conformation compared to RNAP-bound σ^{70}. (**d**) BS^3 and (**e**) DMTMM cross-links displayed on the rank 1 relaxed model. Blue and red – cross-links recovered distances that are within or are not within the C_α-C_α distance covered by the crosslinker, respectively.

***In vivo* CL-MS identifies structural features of the compact apo-σ^{70} conformation**

To explore whether unique features of the predominant compact conformation of apo-σ^{70} exist in living *E. coli* cells, we perform *in vivo* CL-MS during the logarithmic and stationary phases of bacterial growth. Disuccinimidyl suberate (DSS) is a crosslinker, which shares the same end-to-end length and cross-linking chemistry as BS^3. Yet, unlike BS^3, DSS can passively penetrate through cell membranes, including *E. coli*[63]. During the logarithmic phase, σ^{70} is expected to be found mostly in the RNAP-bound form, due to its engagement in the transcription of house-keeping genes[64]. Conversely, during the stationary phase, σ^{38} replaces σ^{70} in the transcription process, which suggest that most of σ^{70} is in a RNAP-unbound form, potentially in the apo form[65]. Following FDR-based filtration of the *in vivo* CL-MS results (Fig. S3, c), we show that during the logarithmic phase of bacterial growth, cross-links can be explained by the RNAP-bound σ^{70} extended conformation (Fig. 2, c). On the other hand, during the stationary phase, we capture DSS cross-links, which we previously captured *in vitro* for apo-σ^{70} using BS^3, and are found to describe exclusively its predominant compact conformation (Fig. 2, a & d). Out of the 49 *in vitro* cross-links, which we found to be unexplained by PDB structures (Fig. 4, c-d, and Table S2), we recover 11 cross-links *in vivo* using DSS during the stationary phase (Fig. 4, b). The results of western-blot of enriched σ^{70} after *in vivo* DSS cross-linking indicate the cross-linked construct is mostly a monomeric σ^{70} with a small fraction of complexes or oligomers that include σ^{70} as well (Fig. S7). This, in turn, suggests that the majority of the recovered cross-links are a result of conformational changes in the monomeric apo-σ^{70}. The cross-links recovered from *in vivo* CL-MS are summarized in supplementary spreadsheet S1 and are displayed on top of a representative PDB structure of σ^{70} (6P1K; Fig. 4). Our results suggest that this apo-σ^{70} compact structure in *E. coli* can be anticipated not during the logarithmic phase, where housekeeping genes are needed, but rather during stress when the binding of σ^{70} to RNAP is replaced by an alternative σ factor. Furthermore, we analyze the interaction interface of σ^{70} with DNA in the RP_o complex using the PDB structures summarized in Table S2 and the program PISA[66]. We find that part of σR1.2, σR2, σR3 and σR4's DNA interacting residues in the RP_o stage undergo cross-linking in the apo-state using DMTMM, these residues include D96, K392, K493, K593, S389, K462. As mentioned DMTMM is a carboxy to amine coupler active at a distance of up to 16Å (C_α-C_α), hence in apo-state σ^{70} DNA binding residues are less accessible to the solvent and are less likely to form interaction with DNA. Based on our knowledge on the interaction of the transcription complex with promoter DNA, together with the fact that all structures of RNAP-bound full-length σ^{70} documented in the PDB are in the extended conformation, we suggest that the unique compact conformation of apo-σ^{70} might be responsible for the inhibition of DNA-interaction, and hence serve as a conformational switch activated upon binding to RNAP.

Discussion

In this work, we provide evidence that apo-σ^{70} is found predominantly in a compact conformation, in which σR4 is in close proximity to σR2 and σR3. We perform CL-MS and further confirm the compact conformation of apo-σ^{70} both *in vitro* and *in vivo*, under stationary phase of the bacterial growth. Yet, an atomic resolution experimental structure of apo-σ^{70} has not yet been elucidated. CL-MS is a high throughput technique able to recover distance restraints between pairs of residues, from just a few micrograms of protein[48–53].

CL-MS is limited in that it reports solely on pairs of residues that are within a given distance range and not on the pairs of residues that are at longer distances. Yet, we use cross-linkers to cover a variety of inter-residue distances and to increase the accuracy of the suggested compact conformation and attain both short and intermediate range distances. The fragmentation score suggests how many times a certain peptide was detected. Above a threshold fragmentation score of 0.7 the FDR decreases dramatically. Nevertheless, as we show in the western-blot and in SEC-MALS measurements, our filtered cross-link list includes mostly ones that originate from the monomeric apo-σ^{70}, while some cross-links probably originate from high-order oligomers or complexes at lower frequency. Overall, CL-MS results suggest that apo-σ^{70} may attain multiple different compact structural organizations, which are yet to be structurally recorded in the PDB.

Using smFRET, we show that in the presence of relatively high concentrations of promoter dsDNA, apo-σ^{70} remains predominantly in a compact conformation. Interestingly, a small fraction of σ^{70} in solution exhibits a conformation that is slightly less compact, suggesting that DNA binding may occur to some degree and might induce a slight conformational change between σR2 and σR4 towards a slightly open conformation. Therefore, it raises the question of whether or not the extended conformation of σ^{70} exists intrinsically and dynamically in apo form, interchanging between the two conformations. In fact, previous smFRET studies suggested that such intrinsic conformational dynamics may exist in *E. coli* apo-σ^{70} [5]. As previously shown by *Vishwakarma et al.*[37], we measure the distance between σ^{70} regions using FRET efficiencies between a donor dye labeling residue 579 of σR4 and an acceptor dye labeling residue 442 of σR2. Overall, the results point towards a preexisting conformational equilibrium between a predominant compact conformation, and a minorly-populated less compact conformation of apo-σ^{70}. Furthermore, we show that σ^{70} may partially bind dsDNA in the absence of RNAP, and at low affinity (μM), as opposed to DNA binding in the presence of RNAP, which occurs at high affinity (nM). In that respect, it is important to mention that σ^{70} has been reported to bind DNA structures that deviate from the dsDNA one (e.g., ssDNA in aptamers)[45], however not to dsDNA, and not at high affinities. The ability of apo-σ^{70} to bind DNA is predictable since σ^{70} undergoes intrinsic dynamic conformational changes, which slightly open the σR2 and σR4 DNA binding interface. One can speculate that if σ^{70} would bind dsDNA not in the context of RNAP, it would probably bind it nonspecifically, hence the interaction would be unstable and will lead to inefficient transcription initiation. Indeed, our results encourage the hypothesis and show that dsDNA-induced σR2-σR4 conformational changes are small, occur only to a small fraction of σ^{70} molecules, and only at relatively high dsDNA concentrations. Therefore, to regulate the transcription process and allow efficient transcription initiation it is necessary to protect the DNA binding residues of σ^{70} from being exposed, until binding to RNAP occurs. Binding will activate the required conformational change in σ^{70}, which will extend it and expose its DNA-binding residues. Moreover, similar to core RNAP, anti-σ factors bind σ^{70} covering the σR2-σR4 DNA-binding interface[1]. Therefore, the σR2-σR4 interface can serve as a

conformational switch that self-inhibits and sterically protects the inner DNA binding residues from being exposed, until needed.

Next, we captured cross-links *in vivo* using DSS and compared it to the BS^3 cross-links *in vitro*, since they both share similar thresholds. We found similarity in the DSS and BS^3 crosslinks, which were found to be exclusive to the predominant compact conformation of apo-σ^{70}, suggesting that the compact conformation exists also *in vivo*. Importantly, this finding reports on a biologically-relevant event, where apo-σ^{70} exists in living *E. coli* cells at stationary phase. In other words, σ^{70} is found in an unbound state and is not degraded, or at least not in full. Nevertheless, these results were achieved using a high copy number plasmid of σ^{70}, and hence might also be influenced by over-expression effects. Yet, if over-expression would pose a problem, we would expect to observe the unique cross-linking signatures of the compact apo-σ^{70} conformation also in the logarithmic phase since at this stage σ^{70} exist in the cell at high concentration. To confirm that most cross-links arise from conformational changes, we have also shown that the majority of *in vivo* cross-linked purified σ^{70} (i.e., a fraction of 93%) is present in the monomeric form.

In summary, we propose that apo-σ^{70} organizes in a predominant compact conformation, which may lead to self-inhibition of the high-affinity promoter binding capabilities of σ^{70}. Only upon activation by binding to RNAP, a large conformational change is anticipated, which exposes these DNA-binding residues. We provide biological evidence for the existence of the compact apo-σ^{70} conformation in live *E. coli* cells during the stationary phase.

Acknowledgments

The plasmid of the Cys-less σ^{70} from which we prepared the doubly-labeled σ^{70} variant for our smFRET measurements, was provided to us as a gift from the laboratory of Dr. Shimon Weiss, UCLA. We would like to thank Dr. Paul David Harris for consultation regarding mpH^{2}MM analyses of smFRET data. We would like to thank Dr. Shimon Weiss for fruitful discussions and for inspecting the text of this work. Molecular graphics and analyses performed with UCSF ChimeraX, developed by the Resource for Biocomputing, Visualization, and Informatics at the University of California, San Francisco, with support from National Institutes of Health R01-GM129325 and the Office of Cyber Infrastructure and Computational Biology, National Institute of Allergy and Infectious Diseases.

Funding

The Israel Science Foundation grant 1768/15 (NK)
The Israel Science Foundation grant 556/22 (EL)
The National Institute of Health grant R01 GM130942 (EL as a subaward)
Yad Hanadiv scholarship (KJ)

Author contributions

Analytical tools: NK
Protein purification: KJ
Experimental data: KJ, JZ
Analysis of experimental data: KJ, EL
Writing – original draft: EL, KJ
Writing – reviewing & editing: NK, JZ

Competing interests

All authors declare no competing interests

Data and materials availability

SmFRET data – https://doi.org/10.5281/zenodo.7173886[67]. CLMS data – available at Proteomics Identification Database (PRIDE), The structural basis for the self-inhibition of DNA binding by apo-σ^{70} - CLMS data (ebi.ac.uk; PXD037183).

References

1. Burgess, R.R. (2001). Sigma Factors. In, S. Brenner and J. H. B. T.-E. of G. Miller, eds. (Academic Press), pp. 1831–1834. 10.1006/rwgn.2001.1192.
2. Feklístov, A., Sharon, B.D., Darst, S.A., and Gross, C.A. (2014). Bacterial Sigma Factors: A Historical, Structural, and Genomic Perspective. Annu. Rev. Microbiol. *68*, 357–376. 10.1146/annurev-micro-092412-155737.
3. Paget, M.S.B., and Helmann, J.D. (2003). The σ70 family of sigma factors. Genome Biology *4*, 203–203. 10.1186/gb-2003-4-1-203.
4. Murakami, K.S. (2013). X-ray Crystal Structure of Escherichia coli RNA Polymerase σ70 Holoenzyme. Journal of Biological Chemistry *288*, 9126–9134. 10.1074/jbc.M112.430900.
5. Davis, M.C., Kesthely, C.A., Franklin, E.A., and MacLellan, S.R. (2016). The essential activities of the bacterial sigma factor. Canadian Journal of Microbiology *63*, 89–99. 10.1139/cjm-2016-0576.
6. Saecker, R.M., Record, M.T., and deHaseth, P.L. (2011). Mechanism of Bacterial Transcription Initiation: RNA Polymerase - Promoter Binding, Isomerization to Initiation-Competent Open Complexes, and Initiation of RNA Synthesis. Journal of Molecular Biology *412*, 754–771. 10.1016/j.jmb.2011.01.018.
7. Ruff, F.E., Record, T.M., and Artsimovitch, I. (2015). Initial Events in Bacterial Transcription Initiation. Biomolecules *5*. 10.3390/biom5021035.
8. Chen, J., Chiu, C., Gopalkrishnan, S., Chen, A.Y., Olinares, P.D.B., Saecker, R.M., Winkelman, J.T., Maloney, M.F., Chait, B.T., Ross, W., et al. (2020). Stepwise Promoter Melting by Bacterial RNA Polymerase. Molecular Cell *78*, 275-288.e6. 10.1016/j.molcel.2020.02.017.
9. Mazumder, A., Ebright, R.H., and Kapanidis, A.N. (2021). Transcription initiation at a consensus bacterial promoter proceeds via a 'bind-unwind-load-and-lock' mechanism. eLife *10*, e70090–e70090. 10.7554/eLife.70090.
10. Malinen, A.M., Bakermans, J., Aalto-Setälä, E., Blessing, M., Bauer, D.L.V., Parilova, O., Belogurov, G.A., Dulin, D., and Kapanidis, A.N. (2022). Real-Time Single-Molecule Studies of RNA Polymerase–Promoter Open Complex Formation Reveal Substantial Heterogeneity Along the Promoter-Opening Pathway. Journal of Molecular Biology *434*, 167383–167383. 10.1016/j.jmb.2021.167383.
11. Bae, B., Feklistov, A., Lass-Napiorkowska, A., Landick, R., and Darst, S.A. (2015). Structure of a bacterial RNA polymerase holoenzyme open promoter complex. eLife *4*, e08504–e08504. 10.7554/eLife.08504.
12. Helmann, J.D. (2019). Where to begin? Sigma factors and the selectivity of transcription initiation in bacteria. Molecular Microbiology *112*, 335–347. 10.1111/mmi.14309.
13. Missiakas, D., and Raina, S. (1998). The extracytoplasmic function sigma factors: role and regulation. Molecular Microbiology *28*, 1059–1066. 10.1046/j.1365-2958.1998.00865.x.
14. Helmann, J.D. (1999). Anti-sigma factors. Current Opinion in Microbiology *2*, 135–141. 10.1016/S1369-5274(99)80024-1.
15. Paget, M.S. (2015). Bacterial Sigma Factors and Anti-Sigma Factors: Structure, Function and Distribution. Biomolecules *5*. 10.3390/biom5031245.
16. Kang, J.-G., Paget, M.S.B., Seok, Y.-J., Hahn, M.-Y., Bae, J.-B., Hahn, J.-S., Kleanthous, C., Buttner, M.J., and Roe, J.-H. (1999). RsrA, an anti-sigma factor regulated by redox change. The EMBO Journal *18*, 4292–4298. 10.1093/emboj/18.15.4292.

17. Pané-Farré, J., Lewis, R.J., and Stülke, J. (2005). The RsbRST Stress Module in Bacteria: A Signalling System That May Interact with Different Output Modules. Microbial Physiology *9*, 65–76. 10.1159/000088837.
18. Heinrich, J., and Wiegert, T. (2009). Regulated intramembrane proteolysis in the control of extracytoplasmic function sigma factors. Research in Microbiology *160*, 696–703. 10.1016/j.resmic.2009.08.019.
19. Anne, F.-C., Julia, F., Christian, R., Zingg, E.J., Benjamin, G., and A., V.J. (2009). Sigma factor mimicry involved in regulation of general stress response. Proceedings of the National Academy of Sciences *106*, 3467–3472. 10.1073/pnas.0810291106.
20. Mechold, U., Potrykus, K., Murphy, H., Murakami, K.S., and Cashel, M. (2013). Differential regulation by ppGpp versus pppGpp in Escherichia coli. Nucleic Acids Research *41*, 6175–6189. 10.1093/nar/gkt302.
21. Bae, B., Davis, E., Brown, D., Campbell, E.A., Wigneshweraraj, S., and Darst, S.A. (2013). Phage T7 Gp2 inhibition of Escherichia coli RNA polymerase involves misappropriation of σ70 domain 1.1. Proceedings of the National Academy of Sciences *110*, 19772 LP – 19777. 10.1073/pnas.1314576110.
22. Degen, D., Feng, Y., Zhang, Y., Ebright, K.Y., Ebright, Y.W., Gigliotti, M., Vahedian-Movahed, H., Mandal, S., Talaue, M., Connell, N., et al. (2014). Transcription inhibition by the depsipeptide antibiotic salinamide A. eLife *3*, e02451–e02451. 10.7554/eLife.02451.
23. Zuo, Y., and Steitz, T.A. (2015). Crystal Structures of the E. coli Transcription Initiation Complexes with a Complete Bubble. Molecular Cell *58*, 534–540. 10.1016/j.molcel.2015.03.010.
24. Narayanan, A., Vago, F.S., Li, K., Qayyum, M.Z., Yernool, D., Jiang, W., and Murakami, K.S. (2018). Cryo-EM structure of Escherichia coli σ70 RNA polymerase and promoter DNA complex revealed a role of σ non-conserved region during the open complex formation. Journal of Biological Chemistry *293*, 7367–7375. 10.1074/jbc.RA118.002161.
25. Chen, J., Gopalkrishnan, S., Chiu, C., Chen, A.Y., Campbell, E.A., Gourse, R.L., Ross, W., and Darst, S.A. (2019). E. coli TraR allosterically regulates transcription initiation by altering RNA polymerase conformation. eLife *8*. 10.7554/eLife.49375.
26. Wang, F., Shi, J., He, D., Tong, B., Zhang, C., Wen, A., Zhang, Y., Feng, Y., and Lin, W. (2020). Structural basis for transcription inhibition by E. coli SspA. Nucleic Acids Research *48*, 9931–9942. 10.1093/nar/gkaa672.
27. Travis, B.A., Ramsey, K.M., Prezioso, S.M., Tallo, T., Wandzilak, J.M., Hsu, A., Borgnia, M., Bartesaghi, A., Dove, S.L., Brennan, R.G., et al. (2021). Structural Basis for Virulence Activation of Francisella tularensis. Molecular Cell *81*, 139-152.e10. 10.1016/j.molcel.2020.10.035.
28. Shi, J., Wen, A., Jin, S., Gao, B., Huang, Y., and Feng, Y. (2021). Transcription activation by a sliding clamp. Nature Communications *12*, 1131–1131. 10.1038/s41467-021-21392-0.
29. Saecker, R.M., Chen, J., Chiu, C.E., Malone, B., Sotiris, S., Ebrahim, M., Yen, Y.L., Eng, E.T., and Darst, S.A. (2021). Structural origins of Escherichia coli RNA polymerase open promoter complex stability. Proceedings of the National Academy of Sciences *118*, e2112877118–e2112877118. 10.1073/pnas.2112877118.
30. Wang, F., Feng, Y., Shang, Z., and Lin, W. (2021). A unique binding between SspA and RNAP β'NTH across low-GC Gram-negative bacteria facilitates SspA-mediated transcription regulation. Biochemical and Biophysical Research Communications *583*, 86–92. 10.1016/j.bbrc.2021.10.048.

31. Lambert, L.J., Wei, Y., Schirf, V., Demeler, B., and Werner, M.H. (2004). T4 AsiA blocks DNA recognition by remodeling σ70 region 4. The EMBO Journal *23*, 2952–2962. 10.1038/sj.emboj.7600312.
32. Patikoglou, G.A., Westblade, L.F., Campbell, E.A., Lamour, V., Lane, W.J., and Darst, S.A. (2007). Crystal Structure of the Escherichia coli Regulator of σ70, Rsd, in Complex with σ70 Domain 4. Journal of Molecular Biology *372*, 649–659. 10.1016/j.jmb.2007.06.081.
33. Blanco, A.G., Canals, A., Bernués, J., Solà, M., and Coll, M. (2011). The structure of a transcription activation subcomplex reveals how σ70 is recruited to PhoB promoters. The EMBO Journal *30*, 3776–3785. 10.1038/emboj.2011.271.
34. Malhotra, A., Severinova, E., and Darst, S.A. (1996). Crystal Structure of a σ70 Subunit Fragment from E. coli RNA Polymerase. Cell *87*, 127–136. 10.1016/S0092-8674(00)81329-X.
35. Campbell, E.A., Muzzin, O., Chlenov, M., Sun, J.L., Olson, C.A., Weinman, O., Trester-Zedlitz, M.L., and Darst, S.A. (2002). Structure of the Bacterial RNA Polymerase Promoter Specificity σ Subunit. Molecular Cell *9*, 527–539. 10.1016/S1097-2765(02)00470-7.
36. Li, W., Stevenson, C.E.M., Burton, N., Jakimowicz, P., Paget, M.S.B., Buttner, M.J., Lawson, D.M., and Kleanthous, C. (2002). Identification and Structure of the Anti-sigma Factor-binding Domain of the Disulphide-stress Regulated Sigma Factor σR from Streptomyces coelicolor. Journal of Molecular Biology *323*, 225–236. 10.1016/S0022-2836(02)00948-8.
37. Vishwakarma, K.R., Cao, A.-M., Morichaud, Z., Perumal, A.S., Margeat, E., and Brodolin, K. (2018). Single-molecule analysis reveals the mechanism of transcription activation in M. tuberculosis. Science Advances *4*, eaao5498–eaao5498. 10.1126/sciadv.aao5498.
38. Dombroski, A.J., Walter, W.A., Record, M.T.J., Siegele, D.A., and Gross, C.A. (1992). Polypeptides containing highly conserved regions of transcription initiation factor sigma 70 exhibit specificity of binding to promoter DNA. Cell *70*, 501–512. 10.1016/0092-8674(92)90174-b.
39. Dombroski, A.J., Walter, W.A., and Gross, C.A. (1993). Amino-terminal amino acids modulate sigma-factor DNA-binding activity. Genes & development *7*, 2446–2455. 10.1101/gad.7.12a.2446.
40. Schwartz, E.C., Shekhtman, A., Dutta, K., Pratt, M.R., Cowburn, D., Darst, S., and Muir, T.W. (2008). A Full-Length Group 1 Bacterial Sigma Factor Adopts a Compact Structure Incompatible with DNA Binding. Chemistry & Biology *15*, 1091–1103. 10.1016/j.chembiol.2008.09.008.
41. Callaci, S., and Heyduk, T. (1998). Conformation and DNA Binding Properties of a Single-Stranded DNA Binding Region of σ70 Subunit from Escherichia coli RNA Polymerase Are Modulated by an Interaction with the Core Enzyme. Biochemistry *37*, 3312–3320. 10.1021/bi972041m.
42. Callaci, S., Heyduk, E., and Heyduk, T. (1999). Core RNA Polymerase from E. coli Induces a Major Change in the Domain Arrangement of the σ70 Subunit. Molecular Cell *3*, 229–238. 10.1016/S1097-2765(00)80313-5.
43. Gruber, T.M., Markov, D., Sharp, M.M., Young, B.A., Lu, C.Z., Zhong, H.J., Artsimovitch, I., Geszvain, K.M., Arthur, T.M., Burgess, R.R., et al. (2001). Binding of the Initiation Factor σ70 to Core RNA Polymerase Is a Multistep Process. Molecular Cell *8*, 21–31. 10.1016/S1097-2765(01)00292-1.
44. Konstantin, K., Leonid, M., Anita, N.-M., L., D.S., Dragana, R., E., N.B., Ann, H., Tomasz, H., and Konstantin, S. (2002). A Role for Interaction of the RNA Polymerase Flap Domain with the σ Subunit in Promoter Recognition. Science *295*, 855–857. 10.1126/science.1066303.
45. Feklistov, A., Barinova, N., Sevostyanova, A., Heyduk, E., Bass, I., Vvedenskaya, I., Kuznedelov, K., Merkienė, E., Stavrovskaya, E., Klimašauskas, S., et al. (2006). A Basal Promoter Element Recognized

by Free RNA Polymerase σ Subunit Determines Promoter Recognition by RNA Polymerase Holoenzyme. Molecular Cell *23*, 97–107. 10.1016/j.molcel.2006.06.010.

46. Ha, T., Enderle, T., Ogletree, D.F., Chemla, D.S., Selvin, P.R., and Weiss, S. (1996). Probing the Interaction between Two Single Molecules: Fluorescence Resonance Energy Transfer between a Single Donor and a Single Acceptor. Proceedings of the National Academy of Sciences *93*, 6264–6268. 10.1073/pnas.93.13.6264.
47. Lerner, E., Cordes, T., Ingargiola, A., Alhadid, Y., Chung, S., Michalet, X., and Weiss, S. (2018). Toward dynamic structural biology: Two decades of single-molecule Förster resonance energy transfer. Science *359*, eaan1133–eaan1133. 10.1126/science.aan1133.
48. Kalisman, N., Adams, C.M., and Levitt, M. (2012). Subunit order of eukaryotic TRiC/CCT chaperonin by cross-linking, mass spectrometry, and combinatorial homology modeling. Proceedings of the National Academy of Sciences *109*, 2884–2889. 10.1073/pnas.1119472109.
49. Murakami, K., Elmlund, H., Kalisman, N., Bushnell, D.A., Adams, C.M., Azubel, M., Elmlund, D., Levi-Kalisman, Y., Liu, X., Gibbons, B.J., et al. (2013). Architecture of an RNA polymerase II transcription pre-initiation complex. Science *342*. 10.1126/science.1238724.
50. Leitner, A., Joachimiak, L.A., Unverdorben, P., Walzthoeni, T., Frydman, J., Förster, F., and Aebersold, R. (2014). Chemical cross-linking/mass spectrometry targeting acidic residues in proteins and protein complexes. Proceedings of the National Academy of Sciences *111*, 9455 LP – 9460. 10.1073/pnas.1320298111.
51. Walker, R.G., Deng, X., Melchior, J.T., Morris, J., Tso, P., Jones, M.K., Segrest, J.P., Thompson, T.B., and Davidson, W.S. (2014). The Structure of Human Apolipoprotein A-IV as Revealed by Stable Isotope-assisted Cross-linking, Molecular Dynamics, and Small Angle X-ray Scattering. Journal of Biological Chemistry *289*, 5596–5608. 10.1074/jbc.M113.541037.
52. Lima, D.B., Melchior, J.T., Morris, J., Barbosa, V.C., Chamot-Rooke, J., Fioramonte, M., Souza, T.A.C.B., Fischer, J.S.G., Gozzo, F.C., Carvalho, P.C., et al. (2018). Characterization of homodimer interfaces with cross-linking mass spectrometry and isotopically labeled proteins. Nature Protocols *13*, 431–458. 10.1038/nprot.2017.113.
53. Slavin, M., and Kalisman, N. (2018). Structural analysis of protein complexes by cross-linking and mass spectrometry. In Methods in Molecular Biology, J. A. Marsh, ed. (Springer New York), pp. 173–183. 10.1007/978-1-4939-7759-8_11.
54. Lerner, E., Chung, S., Allen, B.L., Wang, S., Lee, J., Lu, S.W., Grimaud, L.W., Ingargiola, A., Michalet, X., Alhadid, Y., et al. (2016). Backtracked and paused transcription initiation intermediate of Escherichia coli RNA polymerase. Proc. Natl. Acad. Sci. U.S.A. *113*, E6562--E6571.
55. Chung, S., Lerner, E., Jin, Y., Kim, S., Alhadid, Y., Grimaud, L.W., Zhang, I.X., Knobler, C.M., Gelbart, W.M., and Weiss, S. (2019). The effect of macromolecular crowding on single-round transcription by Escherichia coli RNA polymerase. Nucleic Acids Research *47*, 1440–1450. 10.1093/nar/gky1277.
56. Harris, P.D., Narducci, A., Gebhardt, C., Cordes, T., Weiss, S., and Lerner, E. (2022). Multi-parameter photon-by-photon hidden Markov modeling. Nature Communications *13*, 1000–1000. 10.1038/s41467-022-28632-x.
57. Kim, S., Streets, A.M., Lin, R.R., Quake, S.R., Weiss, S., and Majumdar, D.S. (2011). High-throughput single-molecule optofluidic analysis. Nature Methods *8*, 242–242.

58. Mukhopadhyay, J., Kapanidis, A.N., Mekler, V., Kortkhonjia, E., Ebright, Y.W., and Ebright, R.H. (2001). Translocation of σ70 with RNA Polymerase during Transcription: Fluorescence Resonance Energy Transfer Assay for Movement Relative to DNA. Cell *106*, 453–463. 10.1016/S0092-8674(01)00464-0.
59. Kahraman, A., Herzog, F., Leitner, A., Rosenberger, G., Aebersold, R., and Malmström, L. (2013). Cross-Link Guided Molecular Modeling with ROSETTA. PLOS ONE *8*, e73411. 10.1371/journal.pone.0073411.
60. Jumper, J., Evans, R., Pritzel, A., Green, T., Figurnov, M., Ronneberger, O., Tunyasuvunakool, K., Bates, R., Žídek, A., Potapenko, A., et al. (2021). Highly accurate protein structure prediction with AlphaFold. Nature *596*, 583–589. 10.1038/s41586-021-03819-2.
61. Varadi, M., Anyango, S., Deshpande, M., Nair, S., Natassia, C., Yordanova, G., Yuan, D., Stroe, O., Wood, G., Laydon, A., et al. (2022). AlphaFold Protein Structure Database: massively expanding the structural coverage of protein-sequence space with high-accuracy models. Nucleic Acids Research *50*, D439–D444. 10.1093/nar/gkab1061.
62. Baek, M., DiMaio, F., Anishchenko, I., Dauparas, J., Ovchinnikov, S., Lee, G.R., Wang, J., Cong, Q., Kinch, L.N., Schaeffer, R.D., et al. (2021). Accurate prediction of protein structures and interactions using a three-track neural network. Science *373*, 871–876. 10.1126/science.abj8754.
63. Ryl, P.S.J., Bohlke-Schneider, M., Lenz, S., Fischer, L., Budzinski, L., Stuiver, M., Mendes, M.M.L., Sinn, L., O'Reilly, F.J., and Rappsilber, J. (2020). In Situ Structural Restraints from Cross-Linking Mass Spectrometry in Human Mitochondria. J. Proteome Res. *19*, 327–336. 10.1021/acs.jproteome.9b00541.
64. Gruber, T.M., and Gross, C.A. (2003). Multiple Sigma Subunits and the Partitioning of Bacterial Transcription Space. Annu. Rev. Microbiol. *57*, 441–466. 10.1146/annurev.micro.57.030502.090913.
65. Landini, P., Egli, T., Wolf, J., and Lacour, S. (2014). sigmaS, a major player in the response to environmental stresses in Escherichia coli: role, regulation and mechanisms of promoter recognition. Environmental Microbiology Reports *6*, 1–13. 10.1111/1758-2229.12112.
66. Krissinel, E., and Henrick, K. (2007). Inference of Macromolecular Assemblies from Crystalline State. Journal of Molecular Biology *372*, 774–797. 10.1016/j.jmb.2007.05.022.
67. Joron, Khalil, Zamel, Joanna, Dvir, Shani, Kalisman, Nir, and Lerner, Eitan (2022). The structural basis for the self-inhibition of DNA binding by apo-σ70 - smFRET raw data and analyses pipeline.
68. Svetlov, V., and Artsimovitch, I. (2015). Purification of Bacterial RNA Polymerase: Tools and Protocols BT - Bacterial Transcriptional Control: Methods and Protocols. In, I. Artsimovitch and T. J. Santangelo, eds. (Springer New York), pp. 13–29. 10.1007/978-1-4939-2392-2_2.
69. Laurence, T.A., Kong, X., Jäger, M., and Weiss, S. (2005). Probing Structural Heterogeneities and Fluctuations of Nucleic Acids and Denatured Proteins. Proceedings of the National Academy of Sciences of the United States of America *102*, 17348–17353. 10.1073/pnas.0508584102.
70. Müller, B.K., Zaychikov, E., Bräuchle, C., and Lamb, D.C. (2005). Pulsed Interleaved Excitation. Biophysical journal *89*, 3508–3522. 10.1529/biophysj.105.064766.
71. Ingargiola, A., Lerner, E., Chung, S., Weiss, S., and Michalet, X. (2016). FRETBursts: An Open Source Toolkit for Analysis of Freely-Diffusing Single-Molecule FRET. PLoS ONE *11*, e0160716–e0160716.
72. Nir, E., Michalet, X., Hamadani, K.M., Laurence, T.A., Neuhauser, D., Kovchegov, Y., and Weiss, S. (2006). Shot-Noise Limited Single-Molecule FRET Histograms: Comparison between Theory and Experiments. The Journal of Physical Chemistry B *110*, 22103–22124. 10.1021/jp063483n.

73. Chen, J., Zaer, S., Drori, P., Zamel, J., Joron, K., Kalisman, N., Lerner, E., and Dokholyan, N.V. (2021). The structural heterogeneity of α-synuclein is governed by several distinct subpopulations with interconversion times slower than milliseconds. Structure. 10.1016/j.str.2021.05.002.
74. Chaudhury, P., Tripp, P., and Albers, S.-V. (2018). Expression, Purification, and Assembly of Archaellum Subcomplexes of Sulfolobus acidocaldarius. In Protein Complex Assembly: Methods and Protocols, J. A. Marsh, ed. (Springer New York), pp. 307–314. 10.1007/978-1-4939-7759-8_19.